The Design and the Implementation of a Wearable Medical Ultrasonic Transceiver for Bladder Volume Monitoring

by

Özgür Deniz Temel

A Dissertation Submitted to the
Graduate School of Sciences and Engineering
in Partial Fulfillment of the Requirements for
the Degree of

Master of Science

in

Electrical and Electronics Engineering

KOÇ ÜNİVERSİTESİ

August 16, 2023

The Design and the Implementation of a Wearable Medical Ultrasonic Transceiver for Bladder Volume Monitoring

Koç University

Graduate School of Sciences and Engineering

This is to certify that I have examined this copy of a master's thesis by

Özgür Deniz Temel

and have found that it is complete and satisfactory in all respects,

and that any and all revisions required by the final

examining committee have been made.

Committee Members:

____

Asst. Prof. *Levent Beker*

____

Asst. Prof. *Murat Kuşcu*

____

Assoc Prof. *Onur Ferhanoğlu*

Date: ______________________________

This thesis is dedicated to my loving family, for their unconditional and invaluable support on every endeavor that I have taken in my life

ABSTRACT

The Design and the Implementation of a Wearable Medical Ultrasonic Transceiver for Bladder Volume Monitoring
Özgür Deniz Temel
Master of Science in Electrical and Electronics Engineering
August 16, 2023

The manuscript presents an innovative solution for continuous bladder volume monitoring outside hospital settings, through a wireless and fully integrated ultrasonic transceiver. The challenges encountered during the design, engineering, and realization of the device have been comprehensively discussed, along with the results that fall into the performance metrics to provide such an health tracking service. The device comprises multiple ultrasonic transducers for A-mode ultrasonic measurements, and the raw data collected from them are processed on different media. The proposed device completes a full loop of bladder volume detection to a visualization on a patient's smartphone, promising accurate and continuous measurement of bladder volume for the first time. The study's in-vitro and in-vivo tests demonstrate the device's reliability and accuracy, indicating its potential for diagnosing and managing lower urinary tract dysfunctions (LUTD). The device's wireless and non-invasive nature makes it a convenient and accessible option for patients and the healthcare providers, representing a significant step towards improving the quality of life for individuals with LUTD. The manuscript also highlights the potential of wearable technology in healthcare, and the development of this device could pave the way for further advancements in this field.

ÖZETÇE

Mesane Hacmi Takibi için Giyilebilir Tıbbi Ultrasonik Alıcı-Vericinin Tasarımı ve Uygulanması

Özgür Deniz Temel
Elektrik ve Elektronik Mühendisliği, Yüksek Lisans
16 Ağustos 2023

İşbu tez kapsamında, hastane dışı ortamlarda kesintisiz biçimde idrar kesesi hacmi takibi için yenilikçi bir çözüm sunan kablosuz bir entegre ultrasonik cihazı sunulmuştur. Cihazın tasarımı, mühendisliği ve gerçekleştirilmesi sırasında karşılaşılan zorluklar, çözümleri ve böylesi bir sağlık servisini hayata geçirmek için aşılan performans yeterlilikleri kapsamlı bir şekilde tartışılmıştır. Cihaz, A-modlu ultrasonik ölçümler için birkaç ultrasonik çevirici ile iletişim halinde bulunur ve idrar kesesi hacmini tahmin etmek için bu çeviricilerden toplanan veriler farklı alanlarda işlenir. Sunulan cihaz, idrar kesesi hacmi tetkikini, işlenmemiş veriden bir hastanın akıllı telefonundan takip edebileceği şekilde görselleştirmeye kadar tüm gerekli işaret işlemelerini yapar ve idrar kesesi hacminin doğru ve sürekli ölçümünü ile bu alanda bir ilk olma niteliği taşır. In-vitro ve in-vivo testlerinde yapılan çalışmalar cihazın güvenilirliğini ve sonuçların doğruluğunu ortaya koyar ve birçok alt idrar yolu bozukluklarının tanısında ve tedavisinde oldukça önemli bir rol oynayan, mesane hacmi bilgisinin en kolay biçimde sağlık personeli ve hastaya ulaştırılması konusundaki potansiyelini gösterir. Cihazın kablosuz ve vücut içi bir uygulama gerektirmeyen yapısı, hastalar ve sağlık hizmeti sağlayıcıları için uygun ve erişilebilir bir seçenek sunar ve bu hastalıklara sahip bireylerin yaşam kalitesini iyileştirmeye yönelik önemli bir adımı temsil eder. Tez, ayrıca sağlıkta giyilebilir teknolojinin gelişmekte olduğunu ve bu cihazın geliştirilmesi ile bu alandaki potensiyeli vurgulamaktadır.

ACKNOWLEDGMENTS

I owe the pleasure for the opportunity of having worked with our sincere professor Mr. Beker, who has always guided us for the better, also with the great team of Bio-Integrated Micro Devices Lab. I also feel inspired and privileged to have Prof. Eminoğlu's and Mr. Akçören's unconditional technical guidance throughout this journey.

TABLE OF CONTENTS

LIST OF TABLES

LIST OF FIGURES

ABBREVIATIONS

AC	Alternating Current
BOM	Bill of Materials
CAD	Computer Aided Design
CMOS	Complementary Metal-Oxide Semiconductor
DRC	Design Rule Check
DSP	Digital Signal Processing
ERC	Electrical Rule Check
ESD	Electrostatic Discharge
EM	Electromagnetic
FPGA	Field Programmable Gate Array
f_T	Transit Frequency
GBW	Gain-Bandwidth Product
LUTD	Lower Urinary Tract Dysfunctions
IQ	Quiescent Current
OPAMP	Operational Amplifier
QFN	Quad-flat No-lead
SOP	Small Outline Package
SPICE	Simulation Program with Integrated Circuit Emphasis
TSSOP	Thin Shrink Small Outline Package

Chapter 1

INTRODUCTION

Lower urinary tract dysfunctions (LUTD) refer to a group of conditions that affect the bladder and urethra, leading to storage and voiding dysfunction [1]. Storage dysfunction includes conditions like overactive bladder, urinary incontinence, and nocturia, whereas voiding dysfunction includes conditions like urinary retention and urinary obstruction. LUTD is a common problem affecting an estimated 2.3 billion people globally in 2018, a number that is increasing, the primary reason being the population aging [2]. The most common causes of LUTD include benign prostate hyperplasia (BPH), neurological disorders like multiple sclerosis and spinal cord injury, and pelvic organ prolapse [3–5]. The mentioned conditions significantly impact a person's quality of life, causing discomfort, pain, and in some cases, severe health complications. For instance, BPH-LUTD alone was estimated to have a global economic burden of over 73 billion in 2019 [6]. In the United States, Medicare spent over 1.5 billion on related services in 2013 [7]. Given the substantial impact of LUTD, effective prevention, diagnosis, and treatment strategies are crucial in managing this common condition.

Lower urinary tract dysfunction (LUTD) typically stems from issues during bladder filling and emptying, making bladder volume monitoring a vital tool for evaluating bladder function [8]. Currently, doctors rely on ultrasound imaging of the bladder as a quick and harmless method to estimate bladder volume and determine post-void residual volume [9]. However, the urodynamic studies that revolve around catheterization and cystometry provide the most accurate measurement of bladder volume, but their invasiveness limits their use to non-routine examinations [10]. For out-of-hospital monitoring, patients use urinary diaries and questionnaires to provide information on micturition frequency and volume [11]. Although research has developed implantable sensors [12–16], these invasive devices may only be suitable for patients with severe symptoms in the future [10]. Though a patient with such severe symptoms might really benefit from utilizing the discussed devices, as shown in Fig. 1.1, the implants typically require a serious medical operation for the assembly of the device in the human body, along with bio-compatibility issues that might arise during the treatment period. Regardless of the implanted device, whether using a sensor [12] that is wirelessly excited or the system as a whole to regulate the bladder itself [13], invasive devices are improper choices for the goal of a continuous and comfortable real-time measurements. In short, given the importance of bladder volume monitoring along with the limitations of patient-filled diaries as well as the motivation to refrain from under-the-skin solutions, there is a need for accurate, continuous, and non-invasive technologies to monitor bladder volume [15].

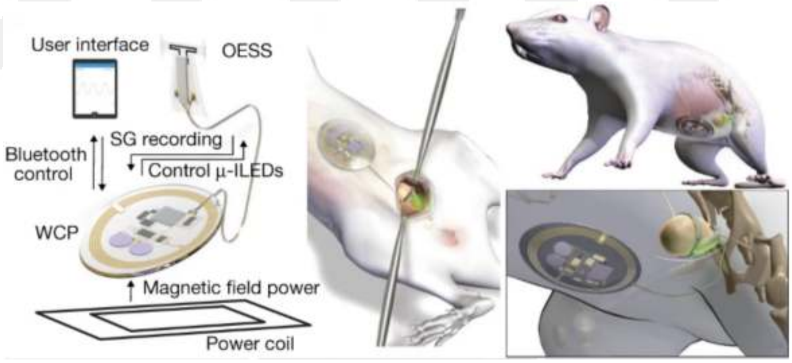

Figure 1.1: An invasive optoelectronic system for optogenetic modulation of bladder function [13]

In order to address LUTD, a great endeavor has been put to expand the wearable devices that can monitor the degree of bladder filling. Three commercial wearable devices, namely Dfree, Novioscan, and Lilium, have been pioneering the field to achieve this objective [17–19]. Though these devices achieve a tremendous job making bladder volume detection accessible, because they rely on signals from the anterior and posterior walls of the bladder to quantify the degree of bladder filling, in spite of being useful in alerting users when their bladders are full, they are not designed for accurate and continuous bladder volume measurement [20–22]. As it has been advertised in [18], which has been illustrated in Fig. 1.2, the corresponding device in the market is useful in the context of estimating the bladder filling, not actually providing an accurate volume detection for the prescription. For that reason, the target communities of these products are kids and elderly citizens, the age group in which lower urinal filling sensing is much more common than the other age groups. In addition, these devices suffer from reliability issues and require ultrasound gel for proper signal transmission [23, 24]. Recently, there have been studies that reported improved accuracy to address such needs for continuous bladder volume measurement. However, the downside of these studies is that they either incorporate bulky electronics subsystems or lack such systems completely [25–29]. Other methods reported in literature include electrical impedance analysis and near-infrared spectroscopy [30–36]. These methods could provide preventative insights, but they are indirect and only suitable for coarse estimations of bladder volume just like their previously discussed commercialized counterparts, mainly due to their low specificity, proneness to motion artifacts, and urine properties [37, 38]. As a result, none of these devices are suitable for accurate and continuous bladder volume monitoring.

Figure 1.2: Commercial bladder filling detector by [18]

All the reported studies with the target of measuring bladder filling, that process ultrasound signals in tiny estates, have proven to be an efficient and convenient alternative solution to current medical treatments while paving the way for the more advanced ones [39]. The advantage of monitoring ultrasounds such as relatively low processing frequencies and non-invasiveness makes them an appealing tool to enable new ways of medical treatment. In a recent study [40], utilizing the Doppler effect in the moving objects, ultrasound waves have been used to scan the moving particles in the deep while a machine learning module helps identify several parameters including central blood pressure, heart rate, and cardiac output, for as long as 12 hours. Similarly, as the fabrication, circuit design, and various learning models in artificial intelligence displays rapid advancement over the past few years, the utilization of these tools happen to have a prime effect on the processing of the ultrasound signals, particularly in medicine [41–43]. For all the discussed reasons, with the new advanced toolset that may accompany the ultrasound waves in medicine, such as deep learning, analog/digital circuit design, and advanced fabrication methods, wearable ultrasound devices has the potential to provide the most convenient healthcare. Given that the combination of all these tools has already begun to enable more accurate and comfortable healthcare, it has become ever so important to contribute to the area to enable new methods of prescription or improve the existing ones.

In order to revolutionize the medical tracking services with the developing technology, considerable research has been published in recent years, that is specific to the field of wearable ultrasonic transducers, along with the hardware and software developments that boost the utilization of such waves, [44–49]. Though the mentioned studies contribute to creating a new dimension in healthcare, reported devices are usually made up of ultrasonic transducers that necessitate bench-top electronics, making it challenging for the patients to receive healthcare outside the hospital settings. As illustrated in Fig. 1.3, although the ultrasound transducers that have been fabricated on a flexible layer, in a phased array configuration is a very promising devices in terms of the transmission accuracy and conformability over the human skin [45], the scenario to realize a single measurement requires a very bulky setup, which makes the transducer to be utilized real-time impossible. In a very similar study, where ultrasound imaging of the cardiac has been discussed over the transducers that have been designed and fabricated for the measurement both in motion and standing still, in spite of the displayed prime transducer performance, the system suffers severely from the integrability, as illustrated in Fig. 1.4.

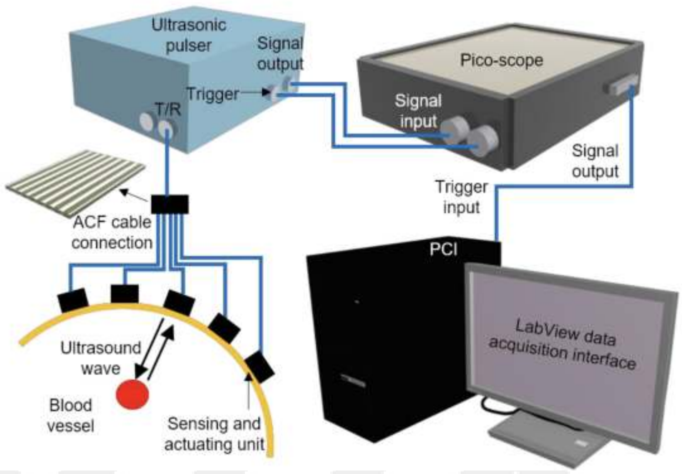

Figure 1.3: Central blood pressure monitoring transducer electronics setup in [46]

In this context, the current devices that are offered both in the market and in the literature suffer from several issues. The existing solutions in the market are convenient, packed, and off the grid, yet they severely lack the ability to accurately quantize the bladder volume and only output an estimate of the degree of the filling [17–19]. The studies that address the accuracy concerns have developed quite advanced transducers that are also conformable, however, they require a very bulky bench-top electronics system in order to fully utilize the performance of the devices that had been developed. The last group of the studies has an invasive approach, however, for continuous and comfortable tracking of the bladder volume their medical complexities, and bio-compatibility concerns, they become the absolute no choice. For the reasons listed, the device introduced in this manuscript points to all the design aspects that the current solutions both in the market and the literature fail to provide, also combining accuracy, continuity, and non-invasiveness within a single design. The proposed device is a wireless and fully integrated ultrasonic transceiver that is embedded with a flexible ultrasonic transducer that enables continuous bladder volume monitoring outside hospital settings. The device comprises

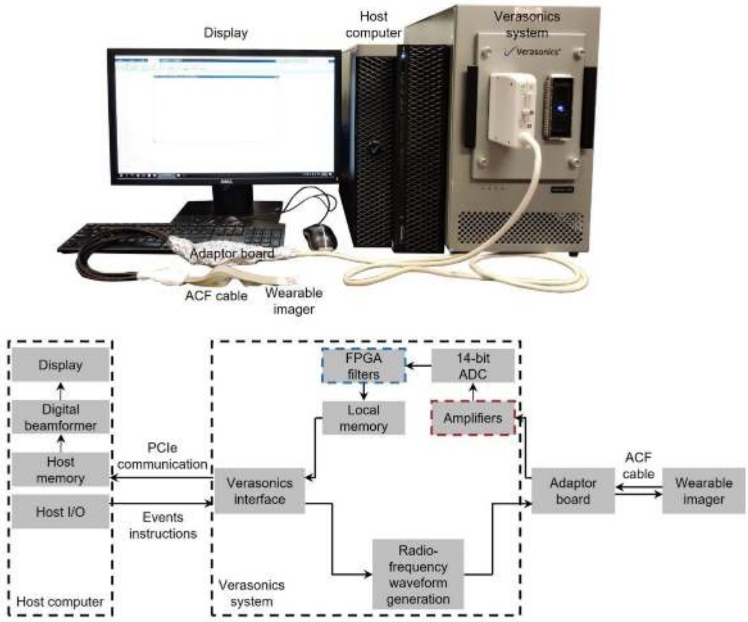

Figure 1.4: Cardiac imaging transducer electronics setup in [47]

several ultrasonic transducers for A-mode ultrasonic measurements and a spherical fitting algorithm for estimating bladder volume, enabling wireless, non-invasive, and precise measurement of bladder volume. While the air-backed design of the ultrasonic transducers makes gel-free measurements possible for people of all ages, an efficient time-of-flight-based measurement avoids the typically intricate computations associated with ultrasonic imaging, allowing the integration of miniaturized electronics for a wearable ultrasonic monitoring system. The whole electronic architecture had been designed and engineered in order to yield the optimum performance for an accurate measurement and realized on a printed circuit board that has been manufactured and tested in the lab environment. The target use case of the device has also been demonstrated, that is connecting the device to a mobile phone via Bluetooth so that bladder volume measurements can be monitored continuously. The performance merits of our device were demonstrated through wireless in-vitro operation in an acoustic setup, along with the wireless in-vivo tests on three healthy young volunteers in order to best mimic the real operation use case of the proposed device.

Given the variety of LUTDs, bladder volume levels being the common indicator of them, the severity of the diseases, along with the challenges in the development of an off-the-grid device; a wearable bladder volume tracking device should pose as an essential tool in the future medicine. The device to alleviate such needs has been presented in this manuscript in the following outline: the first chapter introduces the reader to the issue and presents the motivation and the challenges briefly, the second chapter scans through various designs in the literature, judging these designs in terms of the performance as well as the fracturing the problem into achievable engineering specs, the third chapter explains the design steps, the production steps, the test setups as well as the final results on the electronics bench, as well as some in-vivo results on healthy patients.

Chapter 2

SYSTEM LEVEL DESIGN OF THE DRIVER AND THE READ-OUT

The development of a bladder volume detection device roots its motivation in the severity of the LUTDs and how impactful this method is in addressing this group of diseases. The development of such a device device is a product of collaborative effort from various disciplines. The device as an entire system includes careful designs in terms of the mechanics and acoustics, that serve for a transducer to yield the best performance, as well as a solid supervision of a medical expert is required to examine and judge the results for the most effective prescription, though this currently is at a premature stage to expand the research to. Hence, researchers with various backgrounds are responsible for the solutions for the device from various aspects, which cannot be limited to the mentioned ones only. However, all the developments in the non-electronic areas depend on a reliable electronic design to be meaningful. Therefore to examine the electronics designs in better detail they have also been grouped into different sub-disciplines. The problem of regulating the transducer has three main concerns to be resolved, the driving circuit, the read-out circuit, and the software-related tasks.

2.1 Ultrasonic Transducers

In all the different stages of the design, the transducer performance has been shown to be the performance limiting factor. This led most of the system specs to have been defined around the transducer performance. Therefore, in order to analyze the system the best, it is crucial to address the transducer first. Although the transducer is a very broad term, it usually corresponds to the devices or tools that convert the energy from a given form to another [50]. In this project, it is an ultrasonic transducer, that senses ultrasounds in the environment [51] and accumulates this energy into an electronic charge [52], which is then released into the attached circuit component afterward. All are owed to the phenomenon called piezoelectricity [53]. The transducer under test has a bipolar operation, that is, the same device can be driven with alternating electrical signals to generate mechanical stress, as well as sense mechanical stress to generate such electrical signals. Hence a single device is sufficient for the control.

The measurement technique is another issue related to the transducer, certainly. Various measurement techniques are available and have been in practical use. For example, utilizing the Doppler effect, comparing the amount of the frequency shift of the received signal in a moving environment to the frequency of the excitation signal, one can detect the distance of the object, where the ultrasounds emitted from the source bounces back to the receiver [54]. However, as the operation frequencies elevate, the Doppler shift observed become relatively smaller, which makes the signal detection ever so challenging, as seen in Fig. 2.1. On top of that, ambient noise becomes much more relevant as higher-frequency noises interfere with the spectrum in which the ultrasonic transducers operate. Plus, the bladder volume is a static parameter, that is the amount of urine does not vary during a single measurement cycle. For all the reasons discussed, the measurement technique that fits our application is the time of flight method. The principle is simple and effective, the time between the excitation and the sensing is recorded, which is then used to determine the distance of the object [55], given that the characteristics of the media that the ultrasounds radiate are known.

For all the data collected from the device to be processable as discussed, the received signal has to have high SNR. The primary contributor to a good SNR is the driver indeed. In order to assess the severity of such a concern, the transducers that have been fabricated in our research group have been tested in a pulse-echo experiment, as it had been chosen as the primary method of data acquisition. For the experiment, a single transducer was submerged into a tank filled with deionized water, where the transducer was positioned to face the wall of the water tank. The transducer is excited with a five consecutive burst of pulses with $\pm 5V$ amplitude.

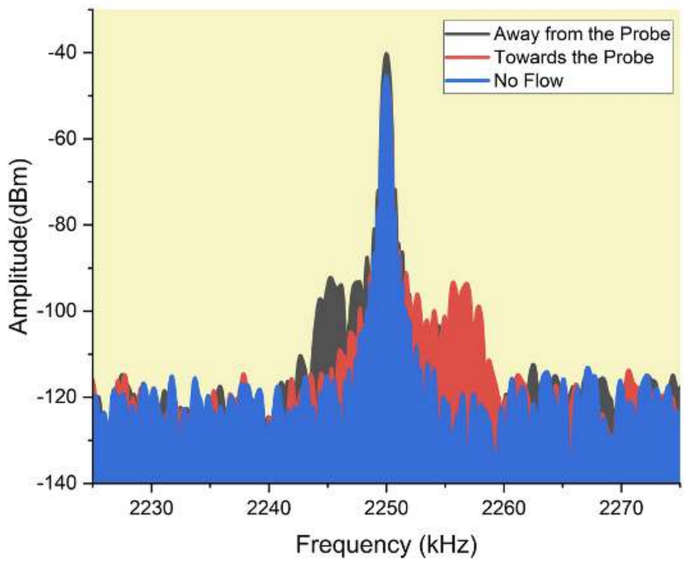

Figure 2.1: Ultrasound patch transducer frequency response

Once the burst is over, the echo signal is routed to the oscilloscope using a diplexer, which has been triggered by the waveform generator that excites the transducer, and the transient in Fig. 2.2 was recorded. It can easily be seen that the ultrasound waves travel back and forth the water tank, and each round of trip has been sensed by the transducer. Though the received signal is somewhat above the noise level, the amplitude is quite insufficient to be sensed by an amplifier. For that reason, the excitation pulses are required to be at higher voltages in order to receive an echo that is sufficiently above the noise floor to be processed.

The ultimate objective of a bladder volume measurement is to extract a 3D view of the bladder so that an accurate estimation could be made. Phased arrays are a very efficient tool to achieve that, which finds use in military, commercial electronics, as well as in medicine. In a reference design, phased arrays of ultrasound transducers are organized to capture a 3D cardiac image [56]. A similar setup is utilized for another medical application, that is to capture the skull, along with a correction technique to make the detection irrelevant from the skull thickness [57]. In order to realize a similar operation, an array of four transducers was employed, all located nearby to target the bladder at different angles. All are sequentially excited within

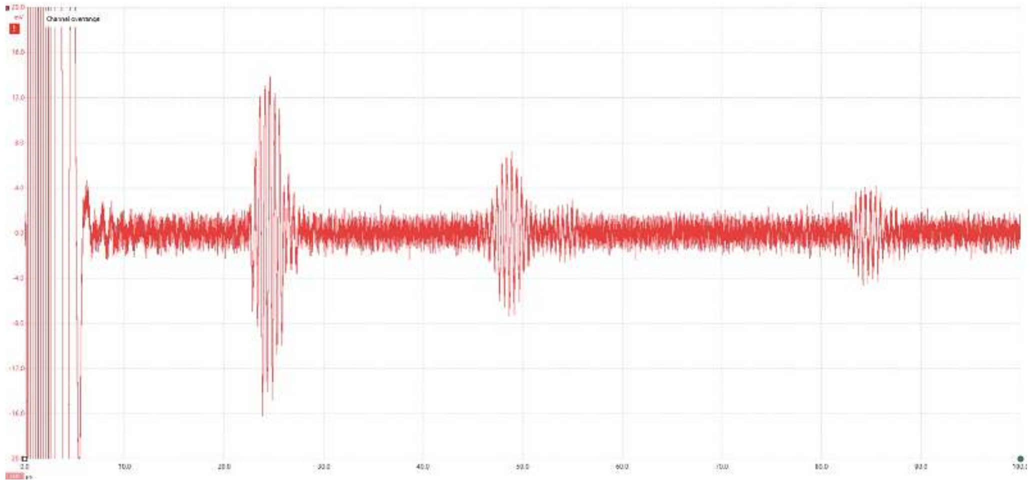

Figure 2.2: Single channel echo transient

a period that is determined to be the repetition rate, in order to prevent any cross-talk between the transducers. The collected data is later fed into a spherical fitting algorithm to estimate the volume.

Taking all the points above into account, the system in Fig. 2.3 has been built to achieve the desired operation. The excitation signals are generated by programming an onboard DSP that is fed into the main driver circuit, where the pulses are conditioned for the transducers. In order to measure the distance reliably with the explained method, each transducer is excited at a rate of 2.5 seconds for a duration of 10 seconds, then the next transducer is excited in the same manner. As coarsely illustrated in Fig. 2.4, a single cycle of measurement was completed within 40 seconds, consequently. The echoes received from the transducers have been selectively directed into the receiver chain according to the described organization. The last but not the least, in order to achieve an off-grid application, various power domains demanded from each block are generated on the same platform. Each block has its own design challenges, therefore each has been discussed in its relative subsections. Nevertheless, one important milestone is to be able to drive the transducers properly, so that the rest of the circuitry receives a meaningful signal to with, for which the next subsection introduces the issues and our solutions for a design of a driver.

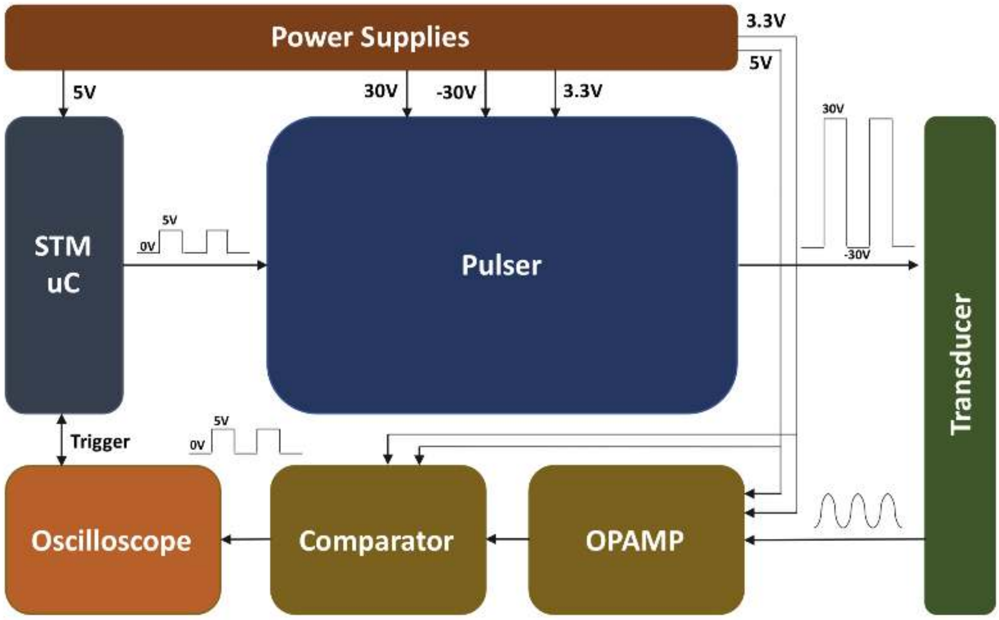

Figure 2.3: Bladder volume tracking device system block diagram

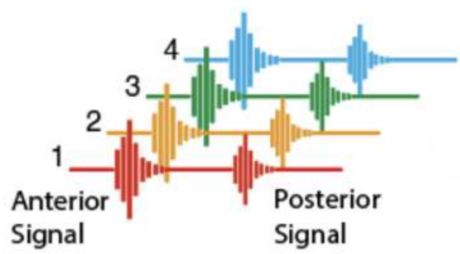

Figure 2.4: Scheme for the measurement of a full cycle

2.2 Driver

The driver is the main block that is responsible for leading the transducer into the action, usually providing an alternating signal to it. Being referred to as the digital front end of the entire system, the driver usually is a compound of various circuits including the components for the control and the sequencing of the pulses, the level shifters that condition these pulses as well as an inverter chain for the final step before the excitation signal arrives at the transducers. All the mentioned circuit types are typically categorized as digital circuits, where signals are processed in two terms as low and high. To illustrate the implementation, in [58] an analog front end (AFE) has been implemented in a single die, consisting of a sequencer that organizes the output pin selection as well as pulse generation over the level shifters, to be used for driving an ultrasound transducer for deep tissue monitoring. Further illustration has also been demonstrated under [59,60] for similar bio-medical applications. The bottom line is that various studies that are recent in this field, utilize an architecture, that is quite similar in terms of the top-level design. In addition to these circuits, there is an auxiliary group of circuits that play a crucial role in the operation of the driver circuit, that is the power management. Yet in this section, it was assumed that the power management is handled ideally and the driver circuit receives noise-free and ripple-free supplies with sufficiently high load regulation capabilities. The function of the first block is a digital signal processing (DSP) block, which is commonly implemented outside the driver package, that is as a standalone chip. For a DSP module, either microcontrollers or field-programmable gate arrays (FPGAs) are quite popularly utilized. Owing to the internal oscillators and phase-locked loops in these DSP blocks, it is possible to generate time-accurate and jitter-free signals, and sequence multiples of them to drive more than a single output in a given timeframe. The digital signals generated in a DSP module have to be operational up to the frequencies that the transducers are operating, which in the framework of the project, is determined to be $2MHz$ based on the frequency analysis performed in Fig. 2.1. This range of frequency is what most DSPs on the shelf are easily compatible with. The conditioned digital signals arrive at a level shifter as the next step. The primary objective is to elevate the voltage level of the incoming signal when the signal is in the high state, and if required to adjust the voltage level during the low state. This circuit achieves this operation by separating the power domains of the input and the output signals, during the conversion. Once the AC signal is elevated to a larger peak-to-peak voltage, the signal is buffered through a chain of inverter stages, in order to improve the transition times between the logic high and the logic low states. With more inverters that the level-shifted signal passes through, shorter transition times are achieved, yet comes with a cost of a larger area, and larger currents that may cause the components to burn. High voltage circuit design strategies are heavily employed in the efforts of developing such parts, in order to ensure safe and reliable operation under extreme supplies that a standard CMOS process usually cannot handle and break down. The level shifters and the inverters circuit are usually internal to the driver circuits, as they usually require less chip estate and can be implemented in multiple channels.

Given that circuit architectures and design perspectives are involved in many integrated circuits, few of them on the shelf are promising in terms of their applications and the specs they promise. MAX14808 has been employed in the final version of the design. The mentioned integrated circuit has many functions inside that have been found to be the most appropriate for our application. To illustrate a few, MAX14808 is a very compact chip in a 10mm X 10mm QFN package, comes with various modes of operations, and as in Fig 2.5 employs an internal digital block to sample and sequence the incoming pulses [61]. The component also operates in 8 different channels, each having its respective input, enabling our system to integrate multiple transducers for 3D bladder measurements. MAX14808 also ensures proper ESD integration though it operates up to $\pm 100V$. The careful ESD design makes the output signal less sensitive to the stray inductances on the PCB, which can easily climb up to a few nH. This provides not only a reliable output, but also a less noisy ground, and enhances the reliability of the internal high-voltage switches. Finally, the driver operation is configured via an on-board STM32 microcontroller from STMicroelectronics [62], that sequences the pulses sent to the MAX14808 driver, along with a reference clock generated by STM32 that is used to sample the input pulses within the driver. All the concerns above constitute an output signal in Fig. 2.3, which illustrates a single channel of the MAX14808, verified on the bench.

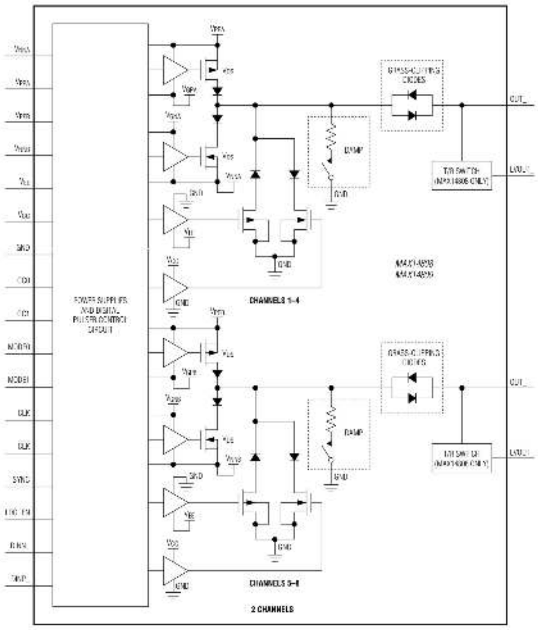

Figure 2.5: MAX14808 pulser top level schematic

When it comes to the application of such high-voltage chips as MAX14808, there are a few concerns that require attention during the PCB design. The pins that are meant to carry currents on the order of amperes have to be addressed and have to be designed to have thicker routes to meet the high current capability requirements. On top of that, what has also been done on the board is to place ceramic caps, that are able to support the voltage ratings required on their respective power rails. As it is also a very good practice to employ both local and remote decoupling caps, namely one in proximity to the PCB pin and one in proximity to the chip's pin for a power rail. This way, the high-frequency resonances caused by the stray inductance and the caps along the rail are significantly dampened. All the mentioned design tricks have been addressed as in Fig. 2.6. Though the MAX14808 covers a significant board estate, the board's floorplan ensures that this chip has the outputs facing outwards the board, the supplies, and the ground on the north of the board to ease the bench work. The last crucial design aspect is to separate the high voltage and the low voltage grounds, that is isolating the driver's ground, although MAX14808 is observed to have an astonishingly silent ground during a single switching activity. All the other components on the board share a common ground, as all operate on a much lower voltage domain. For the PCB design of the other driver component, that is the STM32 microcontroller, the layout design required less engineering and tuning, rather than following the guidelines that the evaluation board of the same chip provides in the component documentation. The layout design of the microcontroller in the end involves a few decoupling capacitors, some pins to be configured with pull-up or pull-down resistors along with implementing the patch antenna as well as its matching circuit on board, which occupies a significantly less board estate.

In a nutshell, in order to boost the power of the echo signal, the transducer has the be driven at higher voltages, which are not as compatible with the standard CMOS chips as additional process steps and reliability concerns are required during the production of these chips, as well as an extended design perspective for their safe application, which also improves the performance of the circuits the operate in a lower voltage domain, which is discussed in the following subsections. In spite of all efforts involved in the handling of such circuits, the echo signal still possesses a limited SNR, which necessitates a careful receiver design. The following section introduces the issues in the analog processing of the echo signal as well as the solutions developed for them.

2.3 Receiver

The receiver circuit as a whole is the primary front end where the echo signals arrive on the board. Although the core of the receiver circuit is the main design target, it is not actually the first stop that the echo signals visit on the board. Following the transducers, that sense the ambient ultrasound echo and convert them to the electrical signals, they are first fed into the output of the MAX14808 back, where the internal transmitter/receiver switch reroutes the signal by breaking the connection of the internal circuit from this output pin and turning on a new connection to

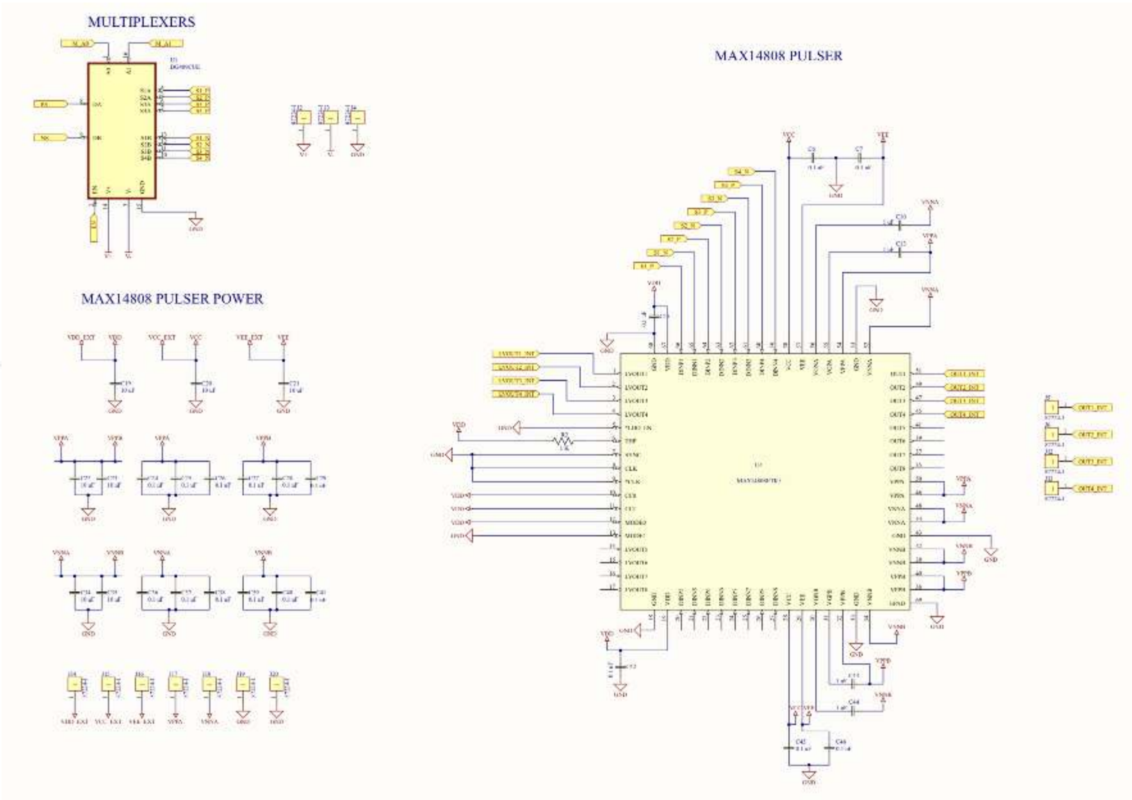

(a) MAX14808 Schematic

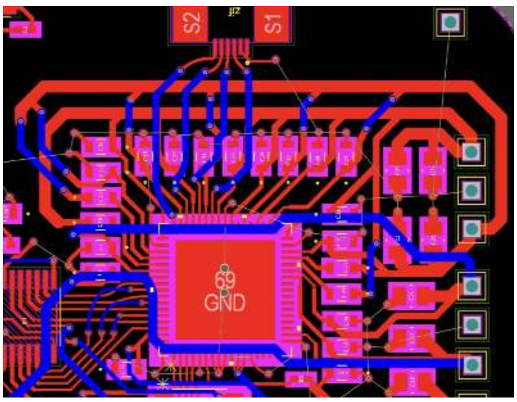

(b) MAX14808 Layout

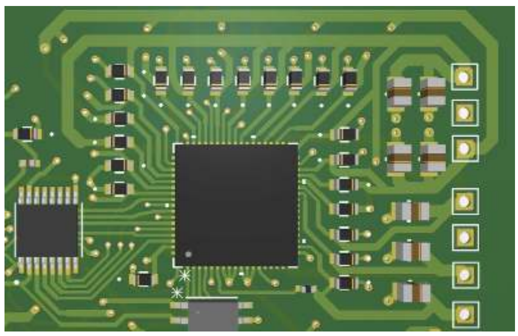

(c) MAX14808 PCB View

Figure 2.6: MAX14808 pulser block level PCB design

another pin of the chip as in Fig. 2.5. The control of this switch is also included in the main sequencing that has been implemented in the microcontroller, as each channel possesses it. Once the echo is directed toward the receiver pin in MAX14808, the signal arrives at a selection stage. The selection stage is a single 3-bit dual analog multiplexer. The component used is DG408 which is composed of 8 different switches that short the input signal to the chip's output based on the selection signal that is encoded into the circuit. The selection of these switches is achieved with the same control signal that programs the transmitter/receiver switches in each channel in the MAX14808. The switches inside DG408 display a very low on-resistance of 100Ω maximum and minimal leakage current of $5nA$ so that the signal is transferred almost without any loss while maintaining a rail-to-rail pass-through [63]. If it was not for this selection stage, each channel had to have its own receiver circuit, which would have caused an extremely large board area, along with a much higher BOM. Without both of these points would have made the board impossible to be integrated into an almost-mobile phone area, and have increased the price of a single part essentially. The signal trespassing the so-called selection stage, the echo finally arrives at an amplifier stage. At this stage, the signal amplitude is tuned to be compatible with the processable levels. This stage is composed of two cascaded low-noise OPAMPs configured in an inverting configuration. The component OPA357 has been specifically hired for this application owing to its low internal noise and high bandwidth of $100MHz$ in open loop and $250MHz$ in unity gain configurations [64]. Other benefits of this product compared to its competitors are the rail-to-rail operation and operating under $3.3V$ to $5V$ supply, being compatible with many of the components on the board. In order to achieve proper amplification, each stage displays a 10-magnitude gain. A single stage with 100 gain has been specifically avoided, and two primary reasons can be described as the following: dividing the gain into two cascaded stages push the bandwidth even further, also in the inverting configuration, such a high gain disturbs the DC bias points of the circuit. Due to its superior bandwidth, the higher harmonics of the echo signal that are collected from the environment are also amplified to some extent. In order to eliminate these higher harmonics, each stage is followed by a low pass filter. Once the echo amplitude is raised higher, it was digitized using an ADC, so that it can be processed in the microcontroller. Owing to the nature of the measurement method, that is time of flight, we only need to know the time point when the echo signal arrives. Therefore using a comparator circuit, the incoming signal is converted into pulses. The component selected is MAX941, which promises a very low quiescent current of 350μ, quite low input offset of $1mV$, and rail-to-rail operation [65]. However, as seen in Fig **??**, the transients of the output of the amplifiers are still chattering owing to the crowded noise content in the incoming echo. To suppress that, an external hysteresis of approximately $0.8V$ is added to the threshold of the comparator with a conventional method explained in [66]. The circuit is set up as in Fig 2.7, and given that the nominal threshold is set to $2.5V$, the falling edge threshold was decreased to $2.5V \times 20K\Omega \,/\, (20K\Omega||60K\Omega) \approx 2.14V$, and the rising edge threshold was increased to $2.5V \times (20K\Omega||60K\Omega) \,/\, 20K\Omega \approx 2.85V$. Note that the mentioned technique is applied at the positive input of the non-inverting comparator, displaying a positive feedback effect. Such described engineering on the receiver circuit completes the measurement loop, namely along with the points addressed in 2.2 the excitation pulse generated in the microcontroller arrives back at the microcontroller, having collected the information of the bladder along the way.

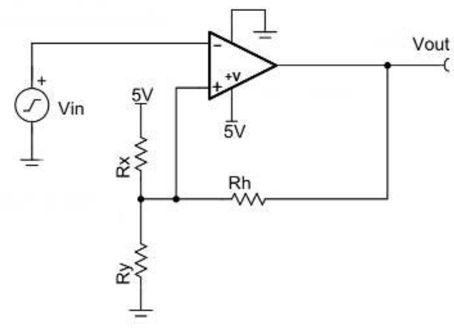

Figure 2.7: Comparator hysteresis

2.4 Power Management

The bladder volume detection board is the combination of various circuits in terms of their targets and design perspectives as explained in the previous sections. Although such a system with such different power requirements has been tried to be designed to have similar supply voltages, there are some circuits that violate the common voltage supply that is provided to the board, which is $5V$. On the driver side, though the STM32 microcontroller operates under $3.3V$ [62], the pulser chip MAX14808 has many different voltages that need to be supplied. The internal pulse generator circuit requires $3.3V$ just like STM32, while the pre-drivers operate between $5V$ and $-5V$, and the pass devices (the output inverter) switch between ± 80 [61]; yet for our application ± 30 suffice to receive an echo signal whose signal power is above the noise floor of the overall system so that it can be processed by the analog front end. Speaking of the receiver side, the default setting for all the components is $5V$, though they can still be operational at $3.3V$ [64, 65]. All the power specifications mentioned called for a very demanding and detailed power management circuit, as each conversion required an additional PMIC component, which was to be the major burden on the BOM of the entire board. Moreover, all the PMIC components came with additional passives such as inductors, capacitors, resistors, and diodes, therefore the layouts of these circuits could have been minimized to a limited extent, which cost as an additional board area. In order to mitigate such an impact, an additional board has been designed, that is to be mounted onto the main board. This board was meant to host the PMIC components only, which had additional advantages such as having been able to have large routes for the rails that carry large currents, given that the second board has an area flexibility. Plus, possible EM interactions that usually are emitted from the PMIC components are avoided. The target organization for all the power management devices for the main board is as follows.

- $5V$ as the global supply and with which the receiver operates
- Buck converter converts the $5V$ input to $3.3V$ for the driver

- Buck converter converts the $5V$ to $2.5V$ that is used as the threshold voltage for the OPAMPs and the comparator in the receiver

- Buck-boost converter with $5V$ input to $-5V$ for MAX14808 pre-drivers.

- Buck-boost converter with $5V$ input to $-30V$ for MAX14808 output stage.

- Boost converter with $5V$ input to $30V$ for MAX14808 output stage.

When it comes to the power consumption of the board all the discussed components so far are assembled. The estimated power consumption for each block is listed in Table 2.1 given that the listed data encapsulates the static currents, as the dynamic currents that are especially quite heavily spent during the switching activities in MAX14808, as well as in the MAX942 comparator [61–65]. The reason why the dynamic currents are neglected is that their duration is limited to few nanoseconds, and during the idle state of the transceiver, that is, after the transducers had been excited and having been waiting for the echoes, there are zero dynamic currents. Provided that a single transducer is excited at every 2.5 seconds with 5 consecutive 2MHz pulses, the idle state corresponds to more than 99.99% of the board's lifetime, effectively averaging the dynamic currents very close to zero within an excitation cycle.

Table 2.1: Static power requirements and supply voltages of the blocks

Block Name	Estimated IQ [mA]	Supply Voltage [V]
STM32wb μC	8mA	3.3V
DG408/9 MUX	5mA	3.3V
MAX14808 HV Pulser	30mA	3.3V-±5V
OPA357 Opamp	5mA	5V
MAX941 Comparator	12mA	5V

The mentioned outline of the power management board has been designed using various components and various architectures. The step-down switching converters, MAX1920, and the step-up converter, MAX5069 have been the final choices in terms of the corresponding PMIC components. The component choices have undergone a few iterations, as even though the specs and an example application have been followed, after a set of simulations with the candidate components if vendors provide SPICE models, the step-up converter circuits in the real application failed to sustain the required load transient and the output voltage has collapsed. The step-down converters have operated very well. Using a single $5V$ supply, the $3.3V$ supply for the STM32 microcontroller and MAX14808 pulser has been generated, along with a $2.5V$ reference for the receiver circuits' threshold voltages. Yet for the step-up converters, although at zero loads, the voltage output can rise above $30V$ for the given resistor combination and the advised large inductance values, during the transducer excitation, the output gradually collapses and the recovery requires a longer time than the excitation duration. The board has been fabricated in spite of the discussed issue persisting in the final design. The strategy on this issue has been not to insist on debugging as it has begun to consume much more effort and time than presumed, continue the experiments with the current setup. Plus, consult an external high voltage supply in case the transducer designs were sub-optimal, and the current produced high voltage on the board hinder the device performance below the target.

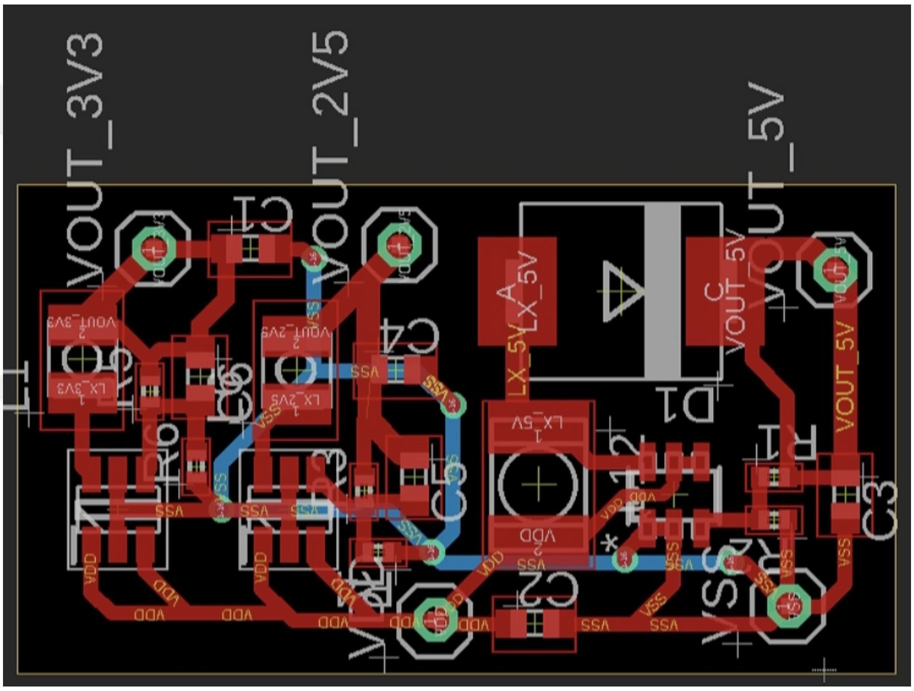

Figure 2.8: Power management board

Chapter 3

REALIZATION, FABRICATION, AND RESULTS

The bladder volume detection board specs and the design for these specs have been comprehensively discussed in chapter 2. In order to enable the patients to be able to utilize the target health care service outside the hospital settings and track their urinal progress without the need for constant medical doctor surveillance, all the discussed designs have to be carefully tested and have to be validated for accurate operation. Therefore to support the theory behind all the designs, each individual component has been tested individually. After successful operation had been achieved in the stand-alone tests, the components are grouped for their roles in the board, which enabled testing the driver, receiver, and power management parts of the entire system in their own units. The last step was to gather all the driver, receiver, and power management modules to form the top-level board to obtain the desired operation of the system. In the given context, the chapter first discusses the methods and the workflow to design the layouts, following that the fabrication and assembly have been discussed. To validate all the discussions, the final results that have been obtained on the bench have been presented lastly.

3.1 Physical Design and Fabrication

The realization of an electronics system composes of several key steps, and physical design and fabrication is certainly one of them. Following defining the circuit topologies and the design parameters associated with the target specs, all the components are carried out to the layout design environment Eagle by Autodesk. For the block-level layout designs, this specific software provides a very intuitive workflow, so that giving its users the opportunity to iterate in their layout designs with minimal effort. In order to be able to design proper layouts in a CAD environment, the footprints of the components are the first and foremost requirement. The mentioned files contain all the required information about the package in which the component has been encapsulated, along with other key information such as pin configuration. To illustrate the workflow of a single board's design, the steps to be explained are utilized. Once the component model had been carefully identified, it has then been imported into the Eagle component library. Specific attention shall be paid to the package information of the downloaded model as any inconsistency between the component currently owned and its model can result in the pins and the chips not fitting into their preserved slot on the board, consequently leading to no proper electrical contact. After ensuring the correct component models, all the connections were set up in Eagle's schematic editor. Later the circuit was carried out to the layout editor where the routes were drawn after deciding on the floorplan. Once the layout design was completed, ERC and DRC tests have been run. These tests ensure that all the connections are matching to the schematic and no dangling nodes exist in the layout, and there are no conditions that might hinder the performance due to fabrication errors, respectively. Although all the block-level designs have been carried out in Eagle, for the more complex top-level layout, the design has been carried over to the Altium software due to its additional functionalities and ease of use for more complex and professional designs. For the top-level design, all the individual block-level schematic and layout have been imported to Altium as in Fig. 3.1, following which the copper lines in between the individual blocks have been routed in the same software's layout editor, where the final version is illustrated in Fig. 3.2. Once all the designs have been completed, the Gerber files were then generated within the software, which contains all the information about the layers, drills, and pin contacts. The last but not the least, the Gerber files that have been transferred to the laser cutter by the company Leiterplatten-Kopierfrasen in the lab, that has been used to print the boards, scratching the copper in FR4 to define the prescribed connections, which finalizes the board design for a sample circuit.

It is certain that alongside the fabrication and physical design methods, the testing conditions are also a critical step in validating the theoretical designs. The steps that have been taken in such validations are intuitive, yet had to be ensured

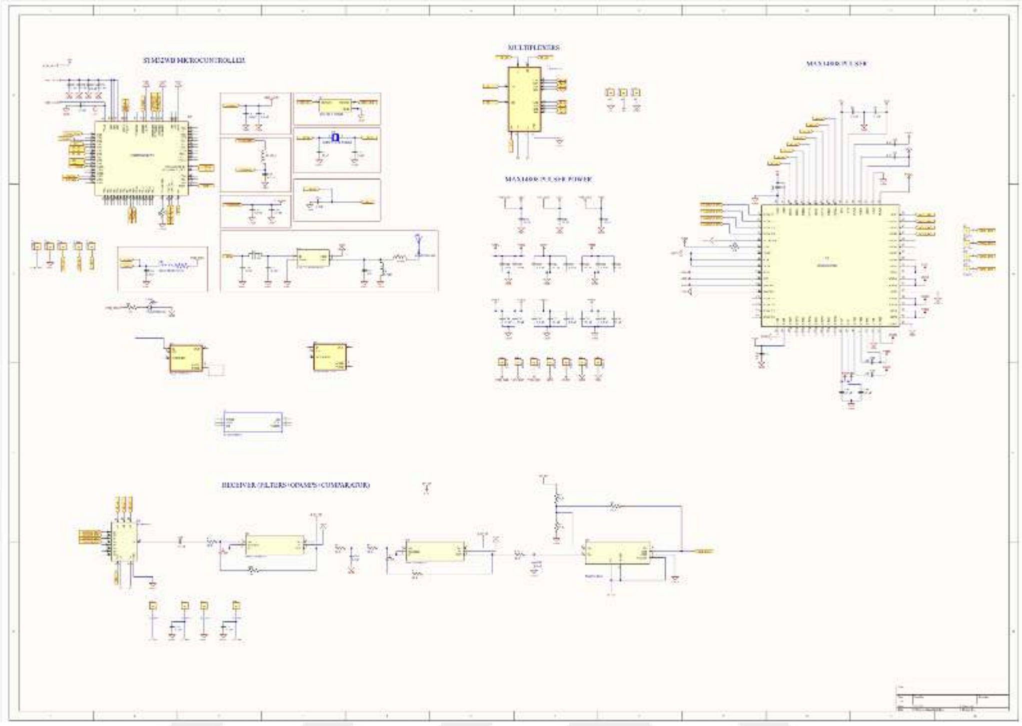

Figure 3.1: Top level schematic

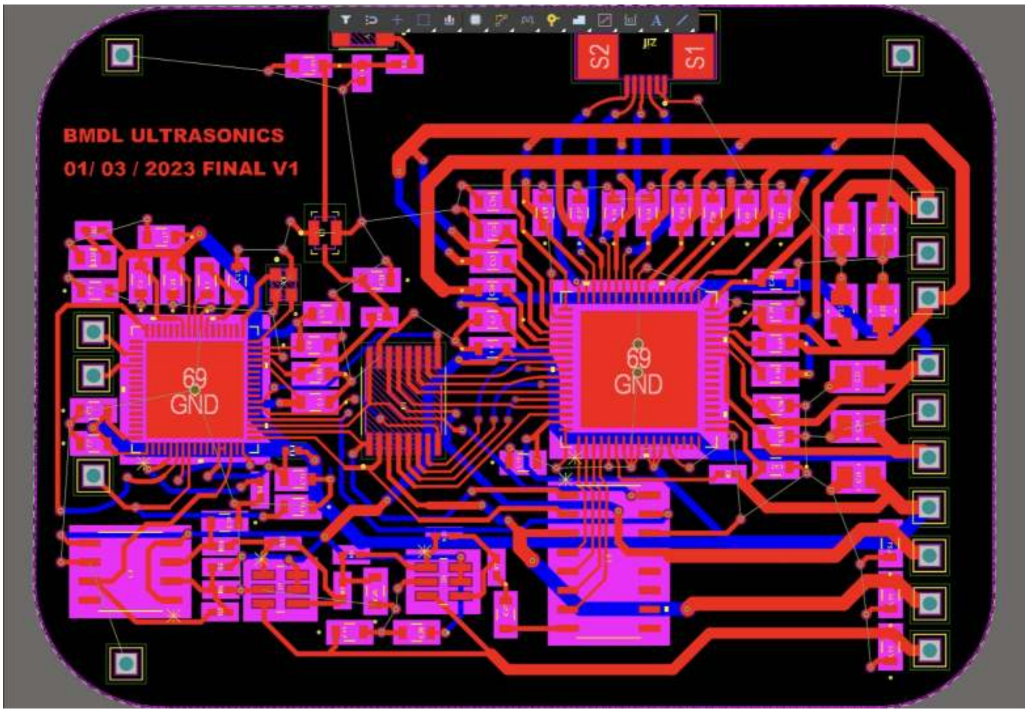

Figure 3.2: Top level layout

for reliable measurements, which include input configuration, building safe connections to the power rails and separating the grounds of corresponding various voltage domains, and probing the required signal with the probes with low capacitance to reduce the loading of the output signals. Though the block level measurements have been acquired with a simple set of instruments, including a waveform generator (Keysight 33500B), power supply (Keithley 2230G), and a digital oscillator (Picoscope 6424E) whose internal ADC has been configured to the highest available number of bits, and sampling rate to the highest allowed that is much larger than our $2MHz$ operation range. On top of that, the top-level measurements have been performed with an additional acoustic setup, which is essentially an aqueous echoic chamber filled with deionized water in which our transducers had been submerged and faced a wall, from which the echo signals returned. All the mentioned bench-top verifications are performed within the lab with the mentioned set of equipment.

Though several steps in the realization and miniaturization of a bladder volume tracking device have been discussed, proper assembly is the last but not the least concern before the final step, which is the actual bench-top tests. In order to put together the circuits that have been designed and fabricated, as in all the discussed steps, all the parts have been assembled within the lab, at the solder station. The key challenges in the assembly have been operating at the correct temperature window with the solder, not so hot to cause damage to the chip packages and legs, as well as the copper PCB routes; also not so cold that the solder melts fast as possible for the most accurate placement of the chips. This has been overcome by using the solder iron in combination with a solder gun, again with an optimized temperature. Another challenge has been having chips with various packages on the same board. For example, the pulse chip was inside a QFN package with an exposed ground pad that has been soldered best using the soldering gun, whereas the components on the receiver side have been in SOP/TSSOP packages that have been soldered fine just using the iron. Therefore for the top-level board, the soldering order had to be engineered so that no component placement disturbs the previously mounted ones. Such an order can coarsely be defined as soldering the large chips, prioritizing the QFN packages, and mounting the passive components around them afterward.

Then the SOP/TSSOP packaged chips have been soldered, and finally the passives around these components. The snapshot of a fully functional board can be seen in Fig. 3.3.

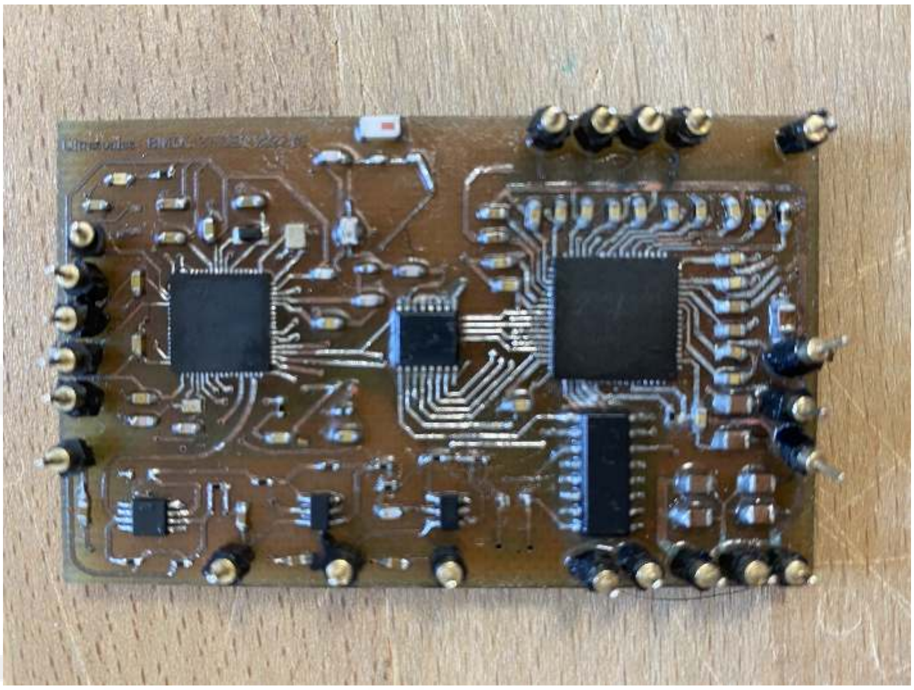

Figure 3.3: Fabricated and assembled board

3.2 Bench and In-vivo Results

In the discipline of microelectronics, although hours are spent in designing and simulating for target specifications, all these efforts solely rely on the mathematical models of the utilized components. More important is whether all the mentioned efforts are true in the end. Therefore it is the last crucial step to verify the circuits post-fabrication to see if both the models and the designs are correct. In order to organize the circuit verifications, they have been split up into different sections, similar to the classifications in chapter 2. First, the analog front-end block has gone through some tests, then the system has been tested as a whole in a pulse-echo experiment. Finally, the device has been shown to be measuring the bladder volume of a patient, while the bladder is almost full and empty.

3.3 Analog Front End

There is a canonical approach in the analog circuit design. Once the models are attained, the circuits are implemented in simulation software, then based on the results, either the design is updated or the circuits are realized. The same approach has been followed during our studies too. First, the SPICE models have been imported in the LTSpice circuit simulator, and then the first two stages of the circuit, which is the amplifier stage in Fig. 3.4 have been implemented. However as in [64], the amplifier models have been generated in their unity feedback mode, and because our simulation setup tries to form a secondary loop around each component in order to realize an inverting OPAMP, a significant mismatch occurred between the simulation results with the bench-top results. For that reason, such simulations have been eliminated from the design process and the circuits were optimized on the bench, given that stability of the feedback loops is guaranteed.

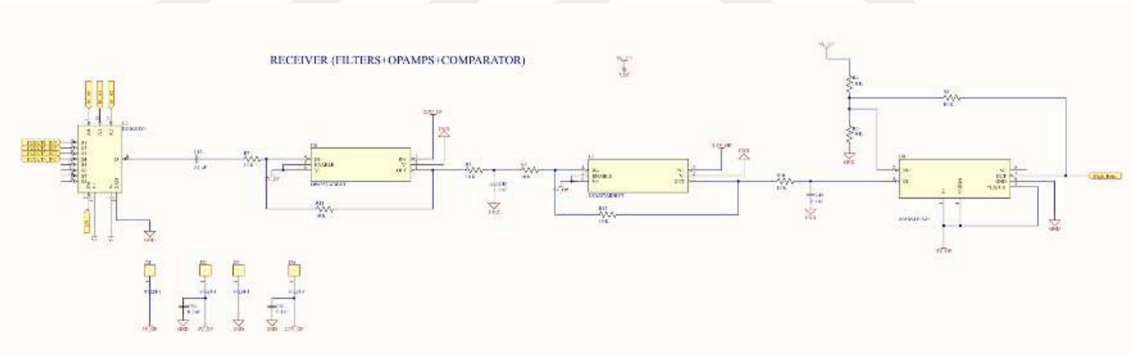

Figure 3.4: Analog front end schematic

In order to assess the stability of an amplifier in negative feedback on the bench, several techniques are present. Observing the small signal response on a transient is a very common method due to its simplicity of it, plus the instruments involved in the test are primary lab equipment that is easily found in a lab. The phase margin, which is the indicator of the loop stability is assessed by observing the settling behavior of the output signal once a small input signal is applied. As explained in [67], once a small step is applied at the input, the output is damped more as the phase margin approaches to 90 deg. Since a phase margin below 45 deg is accepted to be unstable practically, the target output settling is expected to have no overshoot. As seen in Fig. 3.5, the output signal (green) settles with a minimal overshoot to the small input step that has been given in $100mV$ of amplitude around the middle value of the supply range. An additional confirmation to the small signal stability can be discussed in terms of the Barkhasuen criterion [68]. That is, as specified in [64], the amplifier has been designed and tested to be stable under unity gain feedback configuration, therefore as the feedback network gain was increased, the phase margin increased too [68], which takes the loop even further away from oscillation. The glitch in the output signal is to be disregarded as it is purely due to the kickback from the comparator's output (blue). We can safely assume that the amplifier operates around the correct DC bias points with no stability issues.

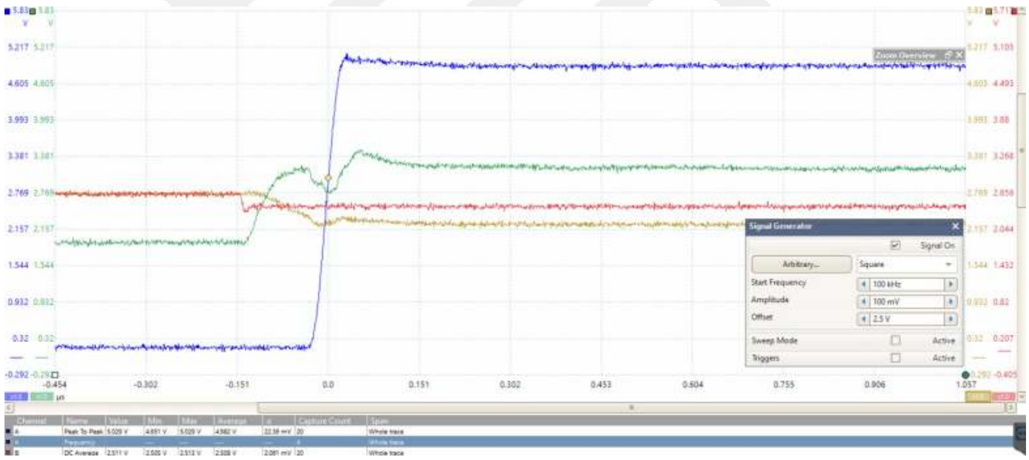

Figure 3.5: Amplifier small signal response

During the assessment of the performance of the AFE in the large signal zone, the amplifier slew rate as well as the comparator internal delay becomes important. Such a test is required in order to ensure that the mentioned parameters are at no such extreme values that can cause a malfunction in the receiver to distort the final measurements. However in Fig. 3.6, it has been shown that the receiver responded very well to the large signal transient, and completed a single acquisition in less the $100\mu s$. This delay was present in each cycle so that it does not bring about a miscalculation in the bladder measurements in the algorithm.

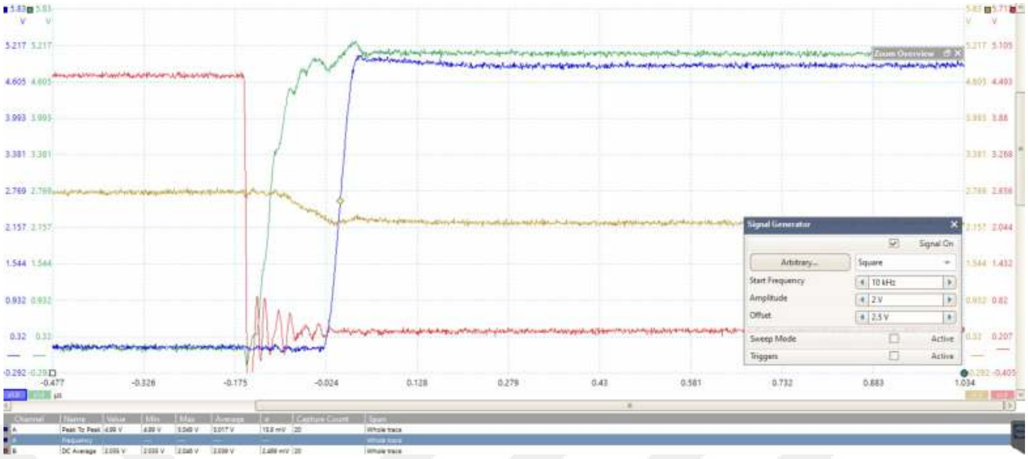

Figure 3.6: Amplifier large signal response

The last but not the least, the analog front end has been fed with an AC signal of a very small amplitude of $200mV$ at $2MHz$ in order to mimic the echo signal that is to be received from a single transducer (red). The input signal is AC-coupled to the desired DC operation point that is around $2.5V$, amplified through the stages to the level that the ADC can differentiate, and lastly digitized. The proper operation of the analog front end has been validated in Fig. 3.7.

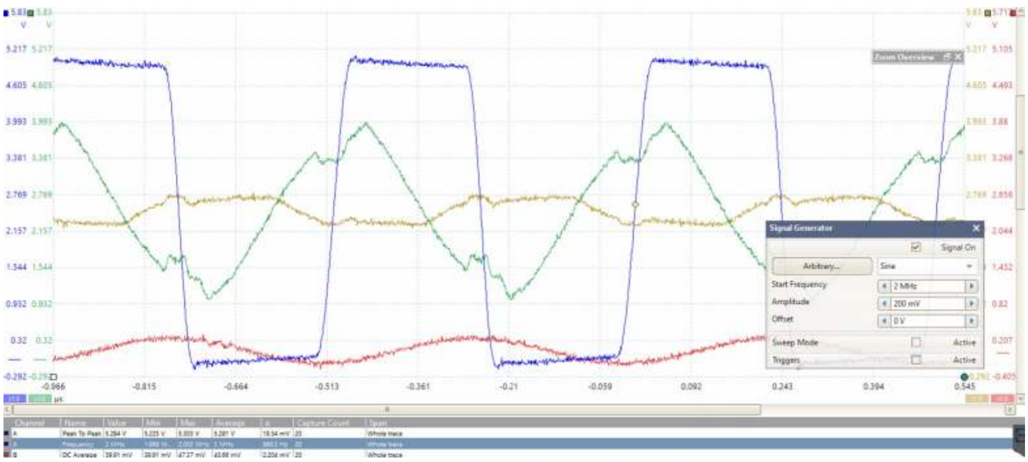

Figure 3.7: Amplifier large signal response

3.4 Pulse-Echo In-vitro and In-vivo Tests

3.4.1 In-vitro Experiments

The AFE has been tested in stand-alone experiments, as well as the microcontroller has been programmed and assembled on the board as in Fig. 3.3, the next step of the verification is the testing of the full loop of the transmitter and receiver structure, for which the number of the external instruments to take a measurement has been significantly reduced to a single oscilloscope along with the power supplies. In order to mimic the bladder, along with the transducer, a beaker has been submerged into the tank filled with deionized water. The beaker has been positioned between the tank wall and the transducer that faces toward the wall. The setup successfully mimics the actual use of the system as the applied ultrasound waves travel at different media during a single measurement cycle. The burst of five pulses that are programmed to oscillate at $2MHz$ was generated in the microcontroller and has been given to the pulser circuit over a multiplexer. Given that the experiment was run with a single transducer, the first channel of the pulser and the multiplexer was selected, so that the microcontroller sends a single selection code to these components during the experiment. Although the echo signal that has been amplified and converted to digital was fed back to the STM32, for the scope of the test, the digital output signal is sensed at the board using a probe. The output signal of the discussed open loop experiment was illustrated in a snapshot at the oscilloscope in Fig. 3.8, where the first group of pulses is the ones that are sensed from the transducer while it is being excited. The second group of pulses are the amplified echos that have been reflected from the anterior wall of the beaker, and the second single pulse is the one that has been reflected from the posterior wall of the beaker. Taking this outcome into account from the practical use point of view, the second echo is naturally much weaker than the first one, yet such signal amplitude depends on the actual position of the bladder, and can easily be compensated by the amplifier gain, provided that the excitation amplitude is at higher voltages. On top of that, the microcontroller is to sense the input from the AFE in an edge-triggered manner, therefore it is to process the time in between the first pulse. Given such a perspective, the output signal in Fig. 3.8 is safe to be processed correctly in the DSP unit, that is the STM32 microcontroller, following which the time of flight data was transferred via an onboard patch antenna, to the mobile application that communicates with the microcontroller over the Bluetooth, where all the calculations and data visualization takes place. For all the reasons discussed above, in order to finalize the assessment of the performance of the bladder volume detection device, the last experiment to be run is an in-vivo test.

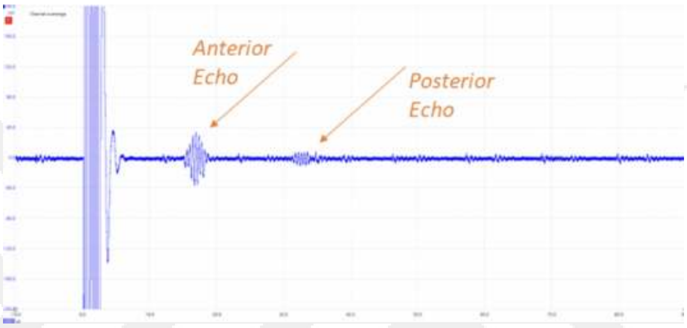

(a) Sensed echo

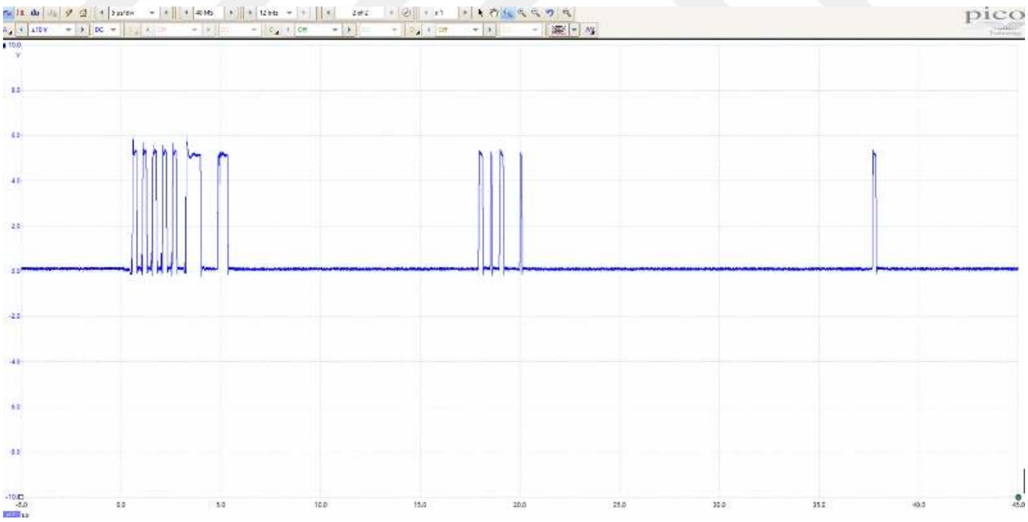

(b) AFE output

Figure 3.8: Single transducer pulse-echo test output

3.4.2 In-vivo Experiments

In-vivo tests of the bladder volume tracking device illustrate how all our developments shall be exercised by a future patient, where the target use case is outside the hospital setting, in the comfort of a patient's home. Therefore these experiments stand as the final assessment for the future use of the device and should address the possible improvements that can be made in the overall system, making way to engineer towards derivatives and the next generations of the device. In spite of the weight of the outcomes of the following experiments, they have been uncomplicated and apparent. This is naturally due to one of the key motivations that the device points to, which is the non-invasive and practical use. To give more insight of the experiment setup, which has been built in the lab, where a volunteering male patient lied and relaxed on. Some experiments in the process of collecting the measurements have been accompanied by a medical doctor only to analyze the outcomes, and no health hazards existed that might have jeopardized the volunteer's well-being. To begin with the experiments, first, the volunteering patient was offered a few glasses of water, simply until he decides that he is not able to take more in. Following a few minutes, the first set of data has been recorded with the patient under the condition that his bladder has been filled considerably. As Fig. 3.9 illustrates, under the test conditions where the transducers, that are external to the board and have a wired connection to it, are excited with five consecutive $2MHz$ pulses with $30V$ amplitude, the echo signals that return from the anterior wall of the bladder as well as from the posterior wall can easily be sensed by our device. Besides, what should also be noted is that for the optimum performance to assess the performance of the transceiver device in the given open loop configuration, single channel operation was preferred and the transducer board has been hovered over near the volunteering patient's bladder to align the transducer board to the patient's bladder.

Once the first set of measurements have been taken, the experiment halted for a brief moment for the patient to get the bladder flushed for the second round. The second set of experiments followed the exact same structure, where the transducer board has again been positioned to the spot where it aligned best with the bladder,

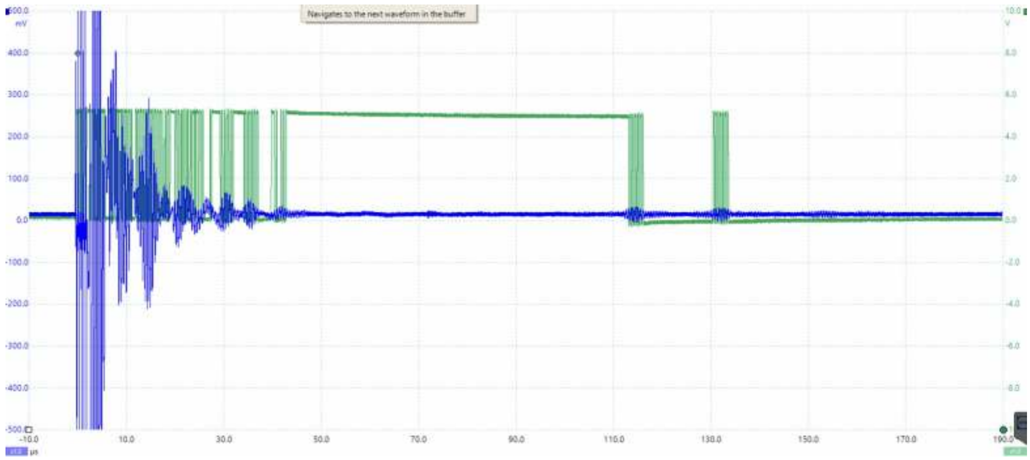

Figure 3.9: AFE input and output with the patient's bladder full

the transducer has been excited with the previous settings via the microcontroller, the device was connected to an external power source, and the output was observed in the open loop manner. At the output of the device, that is the input of the STM32, such plots as in Fig. 3.10 have been recorded. Though the former plot stand-alone does not give a very detailed inside about the amount of the liquid stored within the bladder, compared to the output in Fig. 3.9, the echo from the anterior and the posterior walls are significantly closer and they both make much faster travel through and back the bladder. With both data combined, the valuable message is that the device outputs different transients between the two different states of the bladder, where as the bladder holds more and more liquid, the time of flight returns to a scaled version of the distance taken in the empty state of the bladder.

3.5 Future Perspective

Given all the discussions related to the development of a bladder volume device, a single pocket-sized device has been brought to life from absolute scratch and has been demonstrated on several different tests, each taking a closer step to the real life scenarios, for the first time. The device has been demonstrated to achieve bladder volume measurement in multiple transducers and collect data from each of them in a programmed sequence reliably. The transducers, that have been fabricated

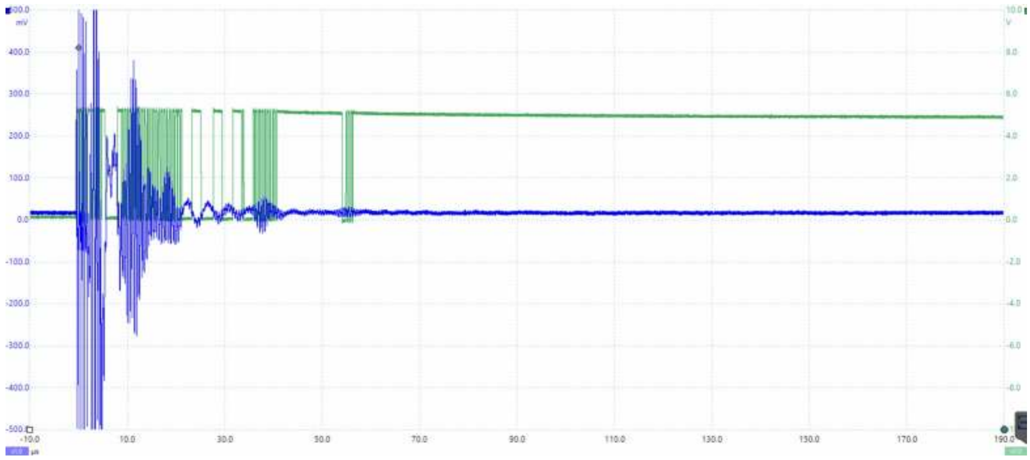

Figure 3.10: AFE input and output with the patient's bladder empty

and optimized in the cleanroom facility of the Koc University have been excited successfully using only the on-board components and the signal has been reliably received and fed back to the on-board DSP unit. Though, in brief terms, such a health service has shown to be enabled, there is always room for development in order to realize an end product. Such potential improvements include a complete set of power management, including a battery with a lifetime for the target measurement period, with which the device still fits the pocket of a pair of trousers. This would definitely be an impactful feature, as it makes the device operate fully off the grid. Another area of improvement can be printing all the components on a flexible PCB and putting it inside a well-designed package, so that a patient can wear the device and continue running all the daily chores, without the anxiety of whether the device has been placed above the bladder at a correct angle. The last area of improvement can be the number of transducers that are excited to collect data. Essentially as there are more channels to collect data from, with more advanced post-processing with the tools including artificial intelligence, the information can be better and more accurately delivered to the medical expert for a more reliable prescription. Yet all the discussed potential improvements revolve around finer engineering, and the evolution of the discussed device, which revolutionizes the treatment of the LUTDs.

Chapter 4

CONCLUSION

In conclusion, lower urinary tract dysfunctions are a common and often debilitating condition affecting millions of people worldwide, with a significant economic burden. Effective prevention, diagnosis, and treatment strategies are crucial in managing this condition. The treatment for many of the LUTDs can be associated with bladder volume, which makes monitoring it a vital tool for evaluating bladder function. Though it is currently carried out through ultrasound imaging or patient-filled diaries, these methods have limitations in terms of the measurement conditions to achieve accurate and continuous information, which raises an urgent need for more accurate, continuous, and non-invasive technologies for monitoring bladder volume. The current solutions offered in the market suffer from either invasiveness, accuracy, or having large electronic setups to make a single measurement. The presented wearable, wireless, and fully integrated ultrasonic transceiver, with a flexible ultrasonic transducer enables continuous bladder volume monitoring outside hospital settings. All the microelectronics architecture including a high voltage driver, a low noise and fast receiver, and power management; along with the data communication for the patient to be able to monitor their urinary conditions on their smartphones, has been designed from scratch, verified with simulation results. Based on the confident designs, the system was realized on a PCB that was fabricated in the lab and the target performance has been achieved on the bench. Then the performance of the miniaturized device was demonstrated through in-vitro and in-vivo tests. With further research and development, this device has the potential to improve the management of LUTD by providing a more reliable and accurate method for monitoring bladder volume continuously and non-invasively. The presented device is a significant step towards meeting the need for accurate, continuous, and non-invasive bladder volume monitoring, and its future development is highly anticipated.

BIBLIOGRAPHY

[1] International Continence Society, “Investigation of LUTS,” Fact Sheet, 2015. [Online]. Available: https://www.ics.org/Wasabi/Documents/DocumentsDownload.aspx?DocumentID=148

[2] T. L. Griebling, “Worldwide prevalence estimates of lower urinary tract symptoms, overactive bladder, urinary incontinence, and bladder outlet obstruction,” *BJU International*, vol. 108, no. 7, pp. 1138–1139, 2011. [Online]. Available: https://doi.org/10.1111/j.1464-410x.2011.10498.x

[3] GBD 2019 Benign Prostatic Hyperplasia Collaborators, “The global, regional, and national burden of benign prostatic hyperplasia in 204 countries and territories from 2000 to 2019: a systematic analysis for the global burden of disease study 2019,” *The Lancet. Healthy longevity*, vol. 3, no. 11, pp. e754–e776, 2022.

[4] V. Phé, E. Chartier-Kastler, and J. N. Panicker, “Management of neurogenic bladder in patients with multiple sclerosis,” *Nature Reviews. Urology*, vol. 13, no. 5, pp. 275–288, 2016.

[5] J. N. Panicker, C. J. Fowler, and T. M. Kessler, “Lower urinary tract dysfunction in the neurological patient: clinical assessment and management,” *The Lancet. Neurology*, vol. 14, no. 7, pp. 720–732, 2015.

[6] L. Feinstein and B. Matlaga, *Urologic diseases in America*, nih publication no. 12–7865 ed. Washington, DC: US Department of Health and Human Services, Public Health Service, National Institutes of Health, National Institute of Diabetes and Digestive and Kidney Diseases, 2018.

[7] B. M. Launer, K. T. McVary, W. A. Ricke, and G. L. Lloyd, “The rising worldwide impact of benign prostatic hyperplasia: The global burden of bph

exceeds all other gu disease," *BJU international*, vol. 127, no. 6, pp. 722–728, 2021.

[8] A. J. Nieuwhof-Leppink, A. J. Klijn, A. Bael, I. Franco, R. A. Hirasing, A. Raes, J. G. Vande Walle, and A. von Gontard, "Daytime urinary incontinence in children and adolescents," *The Lancet. Child & adolescent health*, vol. 3, no. 7, pp. 492–501, 2019.

[9] A. Gammie, O. Finnerty, T. M. Kessler, A. Nambiar, M. Nitschke, R. Pickard, N. Thiruchelvam, H. Tornblom, and M. J. Drake, "What developments are needed to achieve less-invasive urodynamics? ICI-RS 2019," *Neurourology and urodynamics*, vol. 39 Suppl 3, no. S3, pp. S36–S42, 2020.

[10] J. W. Thüroff, P. Abrams, K.-E. Andersson, W. Artibani, C. R. Chapple, M. J. Drake, C. Hampel, A. Neisius, A. Schröder, and A. Tubaro, "EAU guidelines on urinary incontinence," *European Urology*, vol. 59, no. 3, pp. 387–400, 2011.

[11] E. Bright, N. Cotterill, M. J. Drake, and P. Abrams, "Developing and validating the international consultation on incontinence questionnaire bladder diary," *European urology*, vol. 66, no. 2, pp. 294–300, 2014.

[12] S. Mandal, P. Dehghanzadeh, H. Zamani, and S. Shaik, "A wireless implantable microsystem for real-time bladder volume monitoring," 2022. [Online]. Available: https://doi.org/10.36227/techrxiv.20063783.v1

[13] A. D. Mickle, S. M. Won, K. N. Noh, J.-Y. Yoon, K. W. Meacham, Y. Xue, L. A. McIlvried, B. A. Copits, V. K. Samineni, K. E. Crawford *et al.*, "A wireless closed-loop system for optogenetic peripheral neuromodulation," *Nature*, vol. 565, no. 7739, pp. 361–365, 2019.

[14] S. Hannah, J. Hansen, A. Fok, M. Gautheir, S. J. Park, C. McCord, G. Loeb, M.-H. Hsieh, E. T. Hsiao-Wecksler, J. A. Rogers *et al.*, "Conformable, stretchable sensor to record bladder wall stretch," *ACS omega*, vol. 4, no. 1, pp. 1907–1915, 2019.

[15] M. T. Gerber, "Impedance-based bladder sensing," Patent, 2005, uS Patent. [Online]. Available: https://patents.google.com/patent/US9061146B2/en

[16] F. Stauffer, S. Paredes, Y. Zhang, F. Pommereau, S. Santaniello, P.-A. Farine, and H. Shea, "Soft electronic strain sensor with chipless wireless readout: Toward real-time monitoring of bladder volume," *Advanced materials technologies*, vol. 3, no. 6, p. 1800031, 2018.

[17] "Novioscan sens-u kids bladder sensor," Online, 2023. [Online]. Available: https://novioscan.com/

[18] DFree, "DFree wearable device for urinary incontinence," [Online]. Available: https://www.http://dfreeus.biz/, 2023.

[19] Lilium, "Continuous bladder volume monitor," 2023, [Online; accessed 16-April-2023]. [Online]. Available: https://www.lilium.otsuka/en/

[20] P. G. Van Leuteren, A. J. Nieuwhof-Leppink, and P. Dik, "Sens-u: Clinical evaluation of a full-bladder notification–a pilot study," *Journal of pediatric urology*, vol. 15, no. 4, pp. 381.e1–381.e5, 2019.

[21] S. Hofstetter, K. Blod, J. Park, and et al., "Dfree ultrasonic sensor in supporting quality of life and patient satisfaction with bladder dysfunction," *International journal of urological nursing: the journal of the BAUN*, 2022.

[22] J. Kamei, Y. Ikeda, K. Fujita, and T. Nakatani, "Feasibility of approximate measurement of bladder volume in male patients using the lilium α-200 portable ultrasound bladder scanner," *Lower Urinary Tract Symptoms*, vol. 11, no. 3, pp. 169–173, 2019. [Online]. Available: https://onlinelibrary.wiley.com/doi/abs/10.1111/luts.12258

[23] L. Niestoruk, B. Sadowski, and J. Wozniak, "A concept for wearable long-term urinary bladder monitoring with ultrasound. feasibility study," in *2012*

5th European DSP Education and Research Conference (EDERC). IEEE, 2012, pp. 149–153.

[24] F. Semproni, V. Iacovacci, and A. Menciassi, "Bladder monitoring systems: State of the art and future perspectives," *IEEE Access: Practical Innovations, Open Solutions*, vol. 10, pp. 125 626–125 651, 2022.

[25] B. Kiczek, S. Wojcik, W. Bober, S. Hofstetter, S. Müller, A. S. Bhalla, J. R. Smith, P. Ruemmele, D. Althoff, A. Rukosuev *et al.*, "A wearable ultrasonic bladder monitoring device," in *Proceedings of the 28th Annual International Conference on Mobile Computing and Networking.* New York, NY, USA: ACM, 2022, pp. 1–14.

[26] H. G. Jo, H. Kim, H.-M. Kwon, S.-H. Hong, Y. Y. Kim, J. G. Lee, S.-J. Park, and S. S. Lee, "Forward-looking ultrasound wearable scanner system for estimation of urinary bladder volume," *Sensors*, vol. 21, no. 16, p. 5445, 2021.

[27] M. Fournelle, T. Alqaisi, L. Chiou, Y. Gao, P. Rizk, A. Kouba, and A. Goldenberg, "Portable ultrasound research system for use in automated bladder monitoring with machine-learning-based segmentation," *Sensors*, vol. 21, no. 19, p. 6481, 2021.

[28] Q. Gao, Z. Zheng, W. Lu, X. Feng, J. Zhang, Q. Zhang, J. Li, X. Wang, T. Yang, and J. Wu, "Design and development of a bladder volume determination device based on a-mode ultrasound," in *2021 IEEE International Conference on Mechatronics and Automation (ICMA).* IEEE, 2021.

[29] K. Kuru, O. Kuru, V. Tuzlukov, F. Tsow, and Y. Moon, "Intelligent autonomous treatment of bedwetting using non-invasive wearable advanced mechatronics systems and mems sensors: Intelligent autonomous bladder monitoring to treat ne: Intelligent autonomous bladder monitoring to treat ne," *Medical & biological engineering & computing*, vol. 58, no. 5, pp. 943–965, 2020.

[30] V. Gaubert, H. Gidik, and V. Koncar, "Smart underwear, incorporating textrodes, to estimate the bladder volume: proof of concept on a test bench," *Smart Materials & Structures*, vol. 29, no. 8, p. 085028, 2020.

[31] S.-C. Shin, H.-S. Cho, S.-H. Kim, J.-O. Kim, S.-H. Kim, and K.-G. Kim, "Continuous bladder volume monitoring system for wearable applications," in *Annual International Conference of the IEEE Engineering in Medicine and Biology Society. IEEE Engineering in Medicine and Biology Society. Annual International Conference*, 2017, pp. 4435–4438.

[32] T. Schlebusch, P. Borgstrom, M. Jansson, S.-G. Fransson, and F. Seoane, "Bladder volume estimation from electrical impedance tomography," *Physiological measurement*, vol. 35, no. 9, pp. 1813–1823, 2014.

[33] M. Reichmuth, S. Schürle, and M. Magno, "A non-invasive wearable bioimpedance system to wirelessly monitor bladder filling," in *2020 Design, Automation & Test in Europe Conference & Exhibition (DATE)*. IEEE, 2020.

[34] D. Fong, K.-F. Leung, M. Yip, G. Leung, V. Wong, V. Lau, J. Chung, K. Lo, and T. Kwok, "Non-invasive bladder volume sensing for neurogenic bladder dysfunction management," in *2018 IEEE 15th International Conference on Wearable and Implantable Body Sensor Networks (BSN)*. IEEE, 2018.

[35] B. Molavi, J. Lee, R. K. Hampson, Y. Yang, H. Zhu, and A. Saidi, "Noninvasive optical monitoring of bladder filling to capacity using a wireless near infrared spectroscopy device," *IEEE transactions on biomedical circuits and systems*, vol. 8, no. 3, pp. 325–333, 2014.

[36] P. Fechner, D. Y. Lee, J. E. Kim, and J. Kim, "Near-infrared spectroscopy for bladder monitoring: A machine learning approach," *ACM Transactions on Management Information Systems*, vol. 14, no. 2, pp. 1–23, 2023.

[37] A. Koven and S. Herschorn, "NIRS: Past, present, and future in functional

urology," *Current Bladder Dysfunction Reports*, vol. 17, no. 4, pp. 241–249, 2022.

[38] D. Leonhäuser, T. Rappl, M. Schwaibold, J. Fichtner, K. Köhler, and A. Buchner, "Evaluation of electrical impedance tomography for determination of urinary bladder volume: comparison with standard ultrasound methods in healthy volunteers," *Biomedical engineering online*, vol. 17, no. 1, 2018.

[39] J. Powers and F. Kremkau, "Medical ultrasound systems," *Interface focus*, vol. 1, no. 4, pp. 477–489, 2011.

[40] M. Lin, Z. Zhang, X. Gao *et al.*, "A fully integrated wearable ultrasound system to monitor deep tissues in moving subjects," *Nature Biotechnology*, 2023.

[41] S. Liu, Y. Wang, X. Yang, B. Lei, L. Liu, S. X. Li, D. Ni, and T. Wang, "Deep learning in medical ultrasound analysis: a review," *Engineering*, vol. 5, no. 2, pp. 261–275, 2019.

[42] J. Powers and F. Kremkau, "Medical ultrasound systems," *Interface focus*, vol. 1, no. 4, pp. 477–489, 2011.

[43] C. M. Moran and A. J. Thomson, "Preclinical ultrasound imaging—a review of techniques and imaging applications," *Frontiers in Physics*, vol. 8, p. 124, 2020.

[44] H. Hu, N. Shamsudhin, H. Lee, H. Guo, P. Chen, X. Ning, Q. Zhou, Y. Huang, and J. A. Rogers, "Stretchable ultrasonic transducer arrays for three-dimensional imaging on complex surfaces," *Science advances*, vol. 4, no. 3, p. eaar3979, 2018.

[45] C. Wang, X. Li, H. Hu, P. Zhang, Y. Zhang, J. Bai, Q. Zhou, and J. A. Rogers, "Monitoring of the central blood pressure waveform via a conformal ultrasonic device," *Nature biomedical engineering*, vol. 2, no. 9, pp. 687–695, 2018.

[46] C. Wang, B. Qi, M. Lin, Y. Li, Y. Huang, Y. Zhang, S. Wang, H. Zhang, X. Li, T. Zhang *et al.*, "Continuous monitoring of deep-tissue haemodynamics with stretchable ultrasonic phased arrays," *Nat Biomed Eng*, vol. 5, no. 8, pp. 749–758, 2021.

[47] H. Hu, H. Huang, M. Li, and et al., "A wearable cardiac ultrasound imager," *Nature*, vol. 613, no. 7878, pp. 667–675, 2023.

[48] C.-H. Wang, Y. Wu, Y. Liu, Y. Qiao, Y. Chen, S.-E. Lee, Y. Chen, H.-H. Yu, Y.-T. Liu, J. Li *et al.*, "Bioadhesive ultrasound for long-term continuous imaging of diverse organs," *Science*, vol. 377, no. 6605, pp. 517–523, 2022.

[49] F. Wang, Z. Zhu, J. Jiang, Y. Li, Y. Zhang, T. Zhang, Y. Chen, C. Li, Z. Li, L. Li *et al.*, "Flexible doppler ultrasound device for the monitoring of blood flow velocity," *Science advances*, vol. 7, no. 44, p. eabi9283, 2021.

[50] A. Agarwal and J. H. Lang, *Foundations of Analog and Digital Electronic Circuits*. Amsterdam: Elsevier, 2005.

[51] K. Brook, "Ultrasound transducer care and handling tips," *Ultrasound*, 07 2020. [Online]. Available: https://example.com/article-url

[52] F. J. Holler, D. A. Skoog, and S. R. Crouch, *Principles of Instrumental Analysis*, 6th ed. Cengage Learning, 2007.

[53] J. C. Wells, *Longman Pronunciation Dictionary*, 3rd ed. Longman, 2008.

[54] M. Possel, "Waves, motion and frequency: the doppler effect," *Einstein Online*, vol. 5, 2017. [Online]. Available: https://example.com/article-url

[55] A. Devices, "Time of flight," Design Center Glossary, n.d. [Online]. Available: https://www.analog.com/en/design-center/glossary/time-of-flight.html

[56] O. VonRamm and F. Thurstone, "Cardiac imaging using a phased array ultrasound system. i. system design." *Circulation*, vol. 53, no. 2, pp. 258–262, 1976.

[57] S. Smith, G. Trahey, and O. von Ramm, "Phased array ultrasound imaging through planar tissue layers," *Ultrasound in Medicine Biology*, vol. 12, no. 3, pp. 229–243, 1986. [Online]. Available: https://www.sciencedirect.com/science/article/pii/0301562986903145

[58] M. Lin, Z. Zhang, X. Gao *et al.*, "A fully integrated wearable ultrasound system to monitor deep tissues in moving subjects," *Nature Biotechnology*, 2023. [Online]. Available: https://doi.org/10.1038/s41587-023-01800-0

[59] J. M. Rothberg, T. S. Ralston, A. G. Rothberg, J. Martin, J. S. Zahorian, S. A. Alie, N. J. Sanchez, K. Chen, C. Chen, K. Thiele, D. Grosjean, J. Yang, L. Bao, R. Schneider, S. Schaetz, C. Meyer, A. Neben, B. Ryan, J. R. Petrus, J. Lutsky, D. McMahill, G. Corteville, M. R. Hageman, L. Miller, and K. G. Fife, "Ultrasound-on-chip platform for medical imaging, analysis, and collective intelligence," *Proceedings of the National Academy of Sciences*, vol. 118, no. 27, p. e2019339118, 2021. [Online]. Available: https://www.pnas.org/doi/abs/10.1073/pnas.2019339118

[60] "Methods and apparatus for imaging with conformable ultrasound patch," Patent.

[61] Analog Devices Inc., "MAX14808/MAX14809 Datasheet," Datasheet, May 2021, Available at: https://www.analog.com/media/en/technical-documentation/data-sheets/MAX14808-MAX14809.pdf.

[62] STMicroelectronics, "STM32 32-bit Arm Cortex MCUs," Webpage, June 2023, Available at: https://www.st.com/en/microcontrollers-microprocessors/stm32-32-bit-arm-cortex-mcus.html.

[63] Analog Devices Inc., "DG408/DG409 Datasheet," Datasheet, Unknown 2008, Available at: https://www.analog.com/en/products/dg409.html.

[64] Texas Instruments, "OPA357 Datasheet," Datasheet, March 2002, Revised: 2018. Available at: https://www.ti.com/lit/ds/symlink/opa357.pdf?ts=1688424593597.

[65] Analog Devices Inc., "MAX941-MAX944 Datasheet," Datasheet, Unknown 2014, Available at: https://www.analog.com/media/en/technical-documentation/data-sheets/MAX941-MAX944.pdf.

[66] Texas Instruments, "TIDU020A - Understanding the Basic Principles of Wireless Microphone Systems," Technical Document, May 2013, Revised: 2014. Available at: https://www.ti.com/lit/ug/tidu020a/tidu020a.pdf?ts=1688457166118&ref_url=https%253A%252F%252Fwww.google.ro%252F.

[67] D. Meganathan, A. Sukumaran, M. M. D. Babu, S. Moorthi, and R. Deepalakshmi, "A systematic design approach for low-power 10-bit 100 ms/s pipelined adc," *Microelectron. J.*, vol. 40, pp. 1417–1435, 2009.

[68] H. Barkhausen, *Lehrbuch der Elektronen-Röhren und ihrer technischen Anwendungen [Textbook of Electron Tubes and their Technical Applications]*. Leipzig: S. Hirzel, 1935, vol. 3.